2009

Electron-Impact Excitation of O II Fine-Structure Levels

R. Kisielius
Vilnius University, Lithuania

P. J. Storey
University College London, UK

Gary J. Ferland
University of Kentucky, gary@uky.edu

F. P. Keenan
Queen's University Belfast, UK

Mon. Not. R. Astron. Soc. **397,** 903–912 (2009) doi:10.1111/j.1365-2966.2009.14989.x

Electron-impact excitation of O II fine-structure levels★

R. Kisielius,[1]† P. J. Storey,[2] G. J. Ferland[3,4] and F. P. Keenan[5]

[1]*Institute of Theoretical Physics and Astronomy, Vilnius University, A. Goštauto 12, 01108 Vilnius, Lithuania*
[2]*Department of Physics and Astronomy, University College London, Gower Street, London WC1E 6BT*
[3]*Department of Physics, University of Kentucky, Lexington, KY 40506, USA*
[4]*Institute of Astronomy, University of Cambridge, Madingley Road, Cambridge CB3 0HA*
[5]*Astrophysics Research Centre, School of Mathematics and Physics, Queen's University Belfast, Belfast BT7 1NN*

Accepted 2009 April 29. Received 2009 March 30; in original form 2008 October 15

ABSTRACT

Effective collision strengths for forbidden transitions among the five energetically lowest fine-structure levels of O II are calculated in the Breit–Pauli approximation using the R-matrix method. Results are presented for the electron temperature range 100–100 000 K. The accuracy of the calculations is evaluated via the use of different types of radial orbital sets and a different configuration expansion basis for the target wavefunctions. A detailed assessment of previous available data is given, and erroneous results are highlighted. Our results reconfirm the validity of the original Seaton and Osterbrock scaling for the optical O II ratio, a matter of some recent controversy. Finally, we present plasma diagnostic diagrams using the best collision strengths and transition probabilities.

Key words: atomic data – atomic processes – line: formation – planetary nebulae: general.

1 INTRODUCTION

Oxygen ions in different ionization stages are abundant in a wide variety of astrophysical objects, including planetary nebulae, stellar atmospheres, Seyfert galaxies and the interstellar medium. In particular, emission lines arising from transitions among the ground state $1s^22s^22p^3$ levels of O II can be utilized as a diagnostic tool for determining electron density (n_e). Seaton & Osterbrock (1957) suggested the use of the emission doublet-line ratio $I(3729\,\text{Å})/I(3726\,\text{Å})$ of O II arising from nebular transitions from the ground-state levels $^2D_{5/2}$ and $^2D_{3/2}$ to the lowest level $^4S_{3/2}$ as a density indicator. Their work combined Seaton's newly developed collision theories with Osterbrock's access to modern instrumentation to usher in a new era of precision nebular astrophysics (Osterbrock 2000; Osterbrock & Ferland 2006). Osterbrock's observations showed that, in the low-density limit, the observed O II line ratio was equal to the ratio of statistical weights of the upper levels, as expected from Seaton's theories. The O II ratio was the main density indicator for nebulae until improvement in detector technology made the red S II lines accessible. When both nebular and auroral O II transitions (at 7720 and 7730 Å) are considered, both n_e and the electron temperature T_e of the plasma may simultaneously be found, as shown by, for example, Keenan et al. (1999).

To calculate reliable line ratios, one must employ highly accurate atomic data, especially for electron-impact excitation rates and transition probabilities for the forbidden lines. Until the last decade, the most reliable excitation rates for transitions among the $1s^22s^22p^3$ levels of O II have been those of Pradhan (1976), obtained by employing the R-matrix method with inclusion of the five energetically lowest *LS* states, $1s^22s^22p^3\,^4S$, ^2D, ^2P, and $1s^22s2p^4\,^4P$, ^2D. Although the calculation was performed in the non-relativistic approach, the data for the excitation of the fine-structure levels $1s^22s^22p^3\,^2D_{3/2}$, $^2D_{5/2}$ from the ground state $^4S_{3/2}$ were customarily obtained by splitting the non-relativistic values of the excitation rates Υ proportionally to the statistical weights of the final levels, the scaling originally suggested by Seaton & Osterbrock (1957).

However, McLaughlin & Bell (1998) have recalculated excitation rates for O II using the R-matrix method within the Breit–Pauli Breit-Pauli approximation, where the 11 fine-structure levels were included explicitly into a close-coupling formulation of the scattering problem. Their data are significantly different from those of Pradhan (1976), and the differences were attributed to the larger number of states included and a better resolution of the resonance structure in the calculation of McLaughlin & Bell. Subsequently, Keenan et al. (1999) used these newly calculated electron-impact excitation rates in their model to calculate the emission-line ratio diagrams for lines of O II for a range of T_e and n_e appropriate to gaseous nebulae.

More recently, Copetti & Writzl (2002) compared density estimates for planetary nebulae based on different density-indicator lines of O II, S II, Cl III, Ar IV, C III and N I. They found systematic deviations for values of n_e derived from the O II lines, and attributed these to errors in the atomic data, particularly the collision strengths used by Keenan et al. (1999). Furthermore, Wang et al. (2004)

★This paper is dedicated to the memory of Don Osterbrock (1924–2007) and Mike Seaton (1923–2007), who first calibrated the O II density indicator, and did so much to advance the study of nebulae.

†E-mail: R.Kisielius@itpa.lt

have considered four density indicators, including the [O II] λ3729/λ3726 doublet ratio, for a large sample of more than 100 planetary nebulae, and concluded that the calculations of collision strengths by McLaughlin & Bell (1998) are inconsistent with the observations.

Very recently, Montenegro et al. (2006) have investigated relativistic and correlation effects in electron-impact excitation of O II using the Breit-Pauli R-matrix method. They concluded that the fine-structure collision strengths are not affected by relativistic effects and do not significantly depart from the values obtained from a $LS \rightarrow$ LS J transformation. Pradhan et al. (2006) discussed the astrophysical implications of these new atomic data and have derived the O II line ratios $I(3729)/I(3726)$. Their results confirmed analyses of Copetti & Writzl (2002) and Wang et al. (2004). Furthermore, Tayal (2006) and Tayal (2007) have reported similar calculation for O II, employing the B-spline R-matrix method with non-orthogonal sets of radial functions and the inclusion of 47 fine-structure levels. This author also performed a Breit-Pauli R-matrix calculation with orthogonal radial functions involving 62 fine-structure levels in the close-coupling expansion, as an independent check on cross-sections for the forbidden and allowed transitions in O II.

In our work, we study electron-impact excitation of forbidden lines in O II using the R-matrix approach in the Breit-Pauli framework. We attempt to establish if relativistic effects and a sufficient resolution of the resonance structure in the collision strengths can cause the significant departure from the statistical-weight ratio for the Maxwellian-averaged effective collision strengths ϒ, as was claimed in McLaughlin & Bell (1998). Two different sets of configuration basis are employed to describe the target states, in order to evaluate the influence of the number of states included in the scattering problem on the collision strength parameters. Furthermore, we use two different types of radial orbitals (ROs), namely those obtained using Thomas–Fermi–Dirac model potential and Slater-type orbitals, in our scattering calculation. We present a comparison of our calculated energy levels, multiplet oscillator strengths and effective collision strengths obtained using different configuration sets and different ROs with both available experimental data and the theoretical results of other authors.

2 ATOMIC DATA CALCULATION

In the present work, we determine electron-impact collision strengths for the electric-dipole forbidden transitions among the five lowest levels of O II. All possible excitation processes among the fine-structure levels $^4S^o_{3/2}$, $^2D^o_{5/2}$, $^2D^o_{3/2}$, $^2P^o_{3/2}$ and $^2P^o_{1/2}$ of the ground configuration $1s^2 2s^2 2p^3$ are examined using R-matrix close-coupling codes. Collision strengths (Ω) are calculated using a very fine energy mesh for the impact electron energies from the first excitation threshold to the highest threshold, and a coarse energy mesh in the region above all thresholds. These data are thermally averaged for effective collision strengths (ϒ) to be determined in the temperature range 100–100 000 K.

2.1 The scattering target

In the present work, we use two different sets of configuration basis describing the O^+ target states. We include odd configurations $2s^2 2p^3$, $2p^5$, $2s^2 2p^2 \bar{3}p$, $2s^2 2p^2 \bar{4}f$, $2s2p^3 \bar{3}d$, $2p^4 \bar{3}p$, $2s^2 2p \bar{3}p^2$, $2s^2 2p \bar{3}d^2$, $2p^3 \bar{3}d^2$ and even configurations $2s2p^4$, $2s^2 2p^2 3s$, $2s^2 2p^2 \bar{3}d$, $2s2p^3 \bar{3}p$, $2s2p^3 \bar{4}f$, $2p^4 3s$, $2p^4 \bar{3}d$, $2s^2 2p3s\bar{3}p$, $2s2p^2 3s^2$, $2s2p^2 \bar{3}p^2$, $2s2p^2 \bar{3}d^2$, $2s2p^2 3s\bar{3}d$, $2p^3 3s\bar{3}p$ for the basis wavefunction configuration-interaction (CI) expansion in our larger calculation, denoted later as TFD. For the scattering problem only the lowest 11 LS terms are included, which give rise to 21 fine-structure levels. The target wavefunctions are calculated using the general purpose atomic structure code SUPERSTRUCTURE (Eissner, Jones & Nussbaumer 1974; Nussbaumer & Storey 1978). The one-electron radial functions were calculated in adjustable Thomas–Fermi–Dirac model potentials, with the potential scaling parameters λ_{nl} determined by minimizing the sum of the energies of the 11 target states in LS-coupling. In our case, we obtained values for the scaling parameters of $\lambda_{1s} = 1.465$, $\lambda_{2s} = 1.175$, $\lambda_{2p} = 1.129$, $\lambda_{3s} = 1.326$, $\lambda_{\bar{3}p} = -0.785$, $\lambda_{\bar{3}d} = -1.044$, $\lambda_{\bar{4}f} = -1.646$, with the negative values having the significance detailed by Nussbaumer & Storey (1978).

In Table 1, we compare experimental target state energies E_{exp} (Wenåker 1990) with our values E_{TFD} obtained using the above-described wavefunctions for the O^+ target. Energies are presented relative to the ground level $1s^2 2s^2 2p^3 {}^4S^o_{3/2}$. In addition, we list the energy differences $\Delta E_{TFD} = E_{exp} - E_{TFD}$, which were used in the scattering calculation to adjust the theoretical levels so that they match the experimental ones, ensuring a more accurate resonance positioning. There is clearly very good agreement between the calculated and observed energy levels. In most cases, the difference is 1–2 per cent or less, and even for the highest level $1s^2 2s^2 2p^2 3s'' {}^2S^e_{1/2}$ the discrepancy is only 3.9 per cent.

A smaller set consisting of the configurations $2s^2 2p^3$, $2p^5$, $2s^2 2p^2 \bar{3}p$, $2s2p^3 \bar{3}d$, $2s^2 2p \bar{3}p^2$, $2s^2 2p \bar{3}d^2$ for odd symmetries and configurations $2s2p^4$, $2s^2 2p^2 3s$, $2s^2 2p^2 \bar{3}d$, $2s2p^3 \bar{3}p$, $2p^4 3s$, $2p^4 \bar{3}d$, $2s^2 2p3s\bar{3}p$, $2s2p^2 3s^2$, $2s2p^2 \bar{3}p^2$, $2s2p^2 \bar{3}d^2$, $2s2p^2 3s\bar{3}d$ for even symmetries is introduced to replicate the calculation of McLaughlin & Bell (1998), and to check the convergence of our calculations. This set differs from the larger one mainly by the omission of configurations containing the $\bar{4}$f orbital. We use two different sets of one-electron ROs for this set of configurations. In the first, denoted as TFD1, we utilize the same radial functions as in the TFD calculation, while in the second set (denoted as STO1) we use Slater-type ROs obtained by employing the CIV3 code of Hibbert (1975). Their parameters were determined by Bell et al. (1989) for a photoionization calculation, and were used by McLaughlin & Bell (1998) in the electron-impact excitation calculation of O^+.

Similarly to the previous set, only the lowest 11 LS terms yielding 21 fine-structure levels are included in the scattering calculation. Target level energies obtained with this set are denoted as E_{TFD1} and E_{STO1}, and are presented in Table 1 together with the energy differences $\Delta E_{TFD1} = E_{exp} - E_{TFD1}$ and $\Delta E_{STO1} = E_{exp} - E_{STO1}$.

The energy levels calculated by McLaughlin & Bell (1998) are presented in the column E_{MB98} of Table 1. One can see some differences between the level energies E_{STO1} and E_{MB98}, which can be explained by the different number of configuration state functions (CSFs) used in these calculations. We employ a complete set of CSFs arising from the configurations included in the CI wavefunction expansion, whereas McLaughlin & Bell (1998) include a restricted number of CSFs in the wavefunction representation of the O^+ states (for more details see Bell et al. 1989). Finally, in the last column of Table 1 we present the energy levels from Tayal (2007), denoted as (E_{T07}), calculated using non-orthogonal B-spline radial functions. We note that our calculated energy levels for the ground $2s^2 2p^3$ configuration of O II are closer to the experimental values, comparing to the data of Tayal (2007), but this is not true for the levels of excited configurations. Since we are dealing with the transitions within the ground configuration, these deviations do not play a significant role on the accuracy of calculated collision strengths.

One of the ways to estimate the accuracy of chosen wavefunctions is to compare the length and the velocity forms of the multiplet

Table 1. Fine-structure energy levels, their indices N, experimental and calculated energies (Ry) for O II relative to the ground level $2s^22p^3\,^4S^o_{3/2}$.

N	Level	$E_{\rm exp}$	$E_{\rm TFD}$	$\Delta E_{\rm TFD}$	$E_{\rm TFD1}$	$\Delta E_{\rm TFD1}$	$E_{\rm STO1}$	$\Delta E_{\rm STO1}$	$E_{\rm MB98}$	$E_{\rm T07}$
1	$2s^22p^3\,^4S^o_{3/2}$	0.000 00	0.000 00	0.000 00	0.000 00	0.000 00	0.000 00	0.000 00	0.000 00	0.000 00
2	$2s^22p^3\,^2D^o_{5/2}$	0.244 32	0.245 96	−0.001 64	0.259 30	−0.014 98	0.265 19	−0.020 87	0.247 89	0.253 49
3	$2s^22p^3\,^2D^o_{3/2}$	0.244 50	0.245 83	−0.001 33	0.259 16	−0.014 66	0.265 07	−0.020 57	0.247 91	0.253 69
4	$2s^22p^3\,^2P^o_{3/2}$	0.368 77	0.379 11	−0.010 34	0.378 39	−0.009 62	0.386 67	−0.017 90	0.374 13	0.383 89
5	$2s^22p^3\,^2P^o_{1/2}$	0.368 79	0.378 99	−0.010 20	0.378 22	−0.009 43	0.386 53	−0.017 74	0.374 10	0.383 87
6	$2s2p^4\,^4P^e_{5/2}$	1.092 04	1.065 00	0.027 04	1.059 95	0.032 09	1.068 24	0.023 80	1.123 51	1.100 92
7	$2s2p^4\,^4P^e_{3/2}$	1.093 53	1.066 93	0.026 60	1.061 88	0.031 65	1.070 10	0.023 43	1.124 80	1.102 30
8	$2s2p^4\,^4P^e_{1/2}$	1.094 28	1.068 08	0.026 20	1.063 03	0.031 25	1.071 21	0.023 07	1.124 56	1.103 13
9	$2s2p^4\,^2D^e_{5/2}$	1.512 60	1.509 76	0.002 84	1.512 45	0.000 15	1.525 00	−0.012 40	1.546 67	1.543 69
10	$2s2p^4\,^2D^e_{3/2}$	1.512 67	1.509 59	0.003 08	1.512 63	0.000 04	1.524 83	−0.012 16	1.546 60	1.543 75
11	$2s^22p^23s\,^4P^e_{1/2}$	1.687 99	1.697 57	−0.009 58	1.689 90	−0.001 91	1.695 92	−0.007 93	1.677 62	1.691 92
12	$2s^22p^23s\,^4P^e_{3/2}$	1.688 95	1.699 10	−0.010 15	1.691 43	−0.002 48	1.697 36	−0.008 41	1.678 59	1.692 77
13	$2s^22p^23s\,^4P^e_{5/2}$	1.690 39	1.701 63	−0.011 24	1.693 98	−0.003 59	1.699 76	−0.009 37	1.680 21	1.694 18
14	$2s^22p^23s\,^2P^e_{1/2}$	1.721 28	1.742 31	−0.021 03	1.738 82	−0.017 54	1.729 50	−0.008 22	1.725 95	1.726 53
15	$2s^22p^23s\,^2P^e_{3/2}$	1.721 28	1.745 01	−0.023 73	1.741 63	−0.020 35	1.732 19	−0.010 91	1.727 78	1.728 11
16	$2s2p^4\,^2S^e_{1/2}$	1.783 45	1.800 89	−0.017 44	1.796 52	−0.013 07	1.816 21	−0.032 76	1.836 18	1.797 11
17	$2s^22p^23s'\,^2D^e_{5/2}$	1.886 06	1.924 59	−0.038 53	1.916 54	−0.030 48	1.920 18	−0.034 12	1.901 72	1.901 93
18	$2s^22p^23s'\,^2D^e_{3/2}$	1.886 07	1.924 60	−0.038 53	1.916 55	−0.030 48	1.920 18	−0.034 11	1.901 73	1.901 94
19	$2s2p^4\,^2P^e_{3/2}$	1.937 30	1.988 80	−0.051 50	1.989 50	−0.052 20	1.998 60	−0.061 30	2.081 27	1.962 67
20	$2s2p^4\,^2P^e_{1/2}$	1.938 83	1.990 94	−0.052 11	1.991 72	−0.052 89	2.000 82	−0.061 99	2.082 83	1.964 24
21	$2s^22p^23s''\,^2S^e_{1/2}$	2.101 47	2.183 57	−0.082 10	2.183 17	−0.081 70	2.186 39	−0.084 92	2.171 57	2.124 95

Table 2. Comparison of weighted multiplet oscillator strengths in the length ($gf_{\rm L}$) and velocity ($gf_{\rm V}$) forms obtained in our calculation using the SUPERSTRUCTURE code (SS) with the data from Bell et al. (1994) (CIV3) and Tayal (2007) (T07).

Multiplet	SS		CIV3		T07
	$gf_{\rm L}$	$gf_{\rm V}$	$gf_{\rm L}$	$gf_{\rm V}$	$gf_{\rm L}$
$2p^3\,^4S^o$–$2s2p^4\,^4P$	1.068	1.695	1.100	1.240	1.200
$2p^3\,^4S^o$–$2p^23s\,^4P$	0.508	0.450	0.508	0.500	0.448
$2p^3\,^2D^o$–$2s2p^4\,^2D$	1.726	2.251	1.540	1.710	1.820
$2p^3\,^2D^o$–$2p^23s\,^2P$	1.443	1.564	1.200	1.250	1.046
$2p^3\,^2D^o$–$2p^23s\,^2D$	0.542	0.487	0.510	0.510	0.404
$2p^3\,^2D^o$–$2s2p^4\,^2P$	1.791	1.878	1.500	1.600	1.526
$2p^3\,^2P^o$–$2s2p^4\,^2D$	0.235	0.359	0.186	0.222	0.244
$2p^3\,^2P^o$–$2p^23s\,^2P$	0.241	0.282	0.234	0.216	0.240
$2p^3\,^2P^o$–$2s2p^4\,^2S$	0.687	0.811	0.678	0.750	0.528
$2p^3\,^2P^o$–$2p^23s\,^2D$	0.338	0.356	0.270	0.264	0.270
$2p^3\,^2P^o$–$2s2p^4\,^2P$	1.173	1.322	0.516	0.600	0.438
$2p^3\,^2P^o$–$2p^23s\,^2S$	0.062	0.046	0.054	0.060	0.054

oscillator strengths for electric-dipole (E1) transitions calculated in *LS*-coupling. In Table 2, we compare our data with the results from Tayal (2007) (T07) and with those from the more elaborate calculation of Bell et al. (1994) which employs the CIV3 code. Since the latter *gf*-values were obtained in the Breit-Pauli approximation for all lines in the multiplet, we have averaged them in order to obtain oscillator strengths for multiplets. Our calculation was performed using the SUPERSTRUCTURE code of Eissner et al. (1974) in non-relativistic *LS*-coupling. One can see that, in general, there is reasonable agreement between our $gf_{\rm L}$ and $gf_{\rm V}$ values. The $2p^3\,^4S^o$–$2s2p^4\,^4P$ resonance transition shows a greater discrepancy between length and velocity forms, but here the length result is in good agreement with the result of Bell et al. (1994). Indeed, there is generally good agreement between our results and those of Bell et al. (1994) in the length formulation.

The only considerable discrepancy exists for the $2p^3\,^2P^o$–$2s2p^4\,^2P$ multiplet, where the data differ by a factor of 2. There is a similar discrepancy between the two sets of data when we calculate *gf*-values for the fine-structure lines within the Breit-Pauli approximation. Nevertheless, we conclude that the CI wavefunctions employed in our TFD set of calculation are of high accuracy.

2.2 The scattering calculation

We apply the R-matrix method within the Breit-Pauli approximation as described in Burke & Robb (1975), Scott & Burke (1980) and Seaton (1987), and implemented by Berrington et al. (1987) and Berrington, Eissner & Norrington (1995) to compute collision strengths Ω for electron impact on the O^+ ion. In this approach, a non-relativistic Hamiltonian is extended to explicitly include one-electron relativistic terms from the Breit-Pauli Hamiltonian, namely the spin–orbit interaction term, the mass-correction term and the one-electron Darwin term. We use an R-matrix boundary radius of 15.0 au to contain the most diffuse target orbital 3s. The ROs $\overline{3}$p, $\overline{3}$d and $\overline{4}$f describing pseudo-states are orthogonalized to bound orbitals using the Schmidt procedure. Expansion of each scattered electron partial wave is over the basis of 25 continuum wavefunctions within the R-matrix boundary, and the Buttle corrections are added to compensate for the truncation to the finite number of terms in the R-matrix expansion. This allows us to compute accurate collision data for electron energies up to 15 Ry. The partial wave expansion for the $(N+1)$-electron system extends to a maximum total angular momentum $L = 12$ and includes singlet, triplet and quintet *LS* symmetries for both even and odd parities. Subsequently, the Hamiltonian matrices and the long-range potential coefficients obtained in a *LS*-coupling are transformed by means of a unitary transformation to a pair-coupling scheme. The intermediate coupling Hamiltonian matrices are then calculated for the even and odd parities up to a total angular momentum $J = 10$, with the theoretical target level energies adjusted by $\Delta E_{\rm TFD}$ (see Table 1) to ensure

that they match the observed values. We perform the full exchange R-matrix outer region calculation for values of $J = 0{-}10$, and top-up these data for non-dipole allowed transitions assuming that the collision strengths form a geometric progression in J for $J > 10$. In practice, the collision strengths for the transitions between the fine-structure levels are already well converged by $J = 10$.

For example, considering the transition $^4S^o_{3/2}$–$^2D^o_{5/2}$ Ω at the $E = 2.1$ Ry, the partial waves with $J = 0{-}5$ contribute 99.8 per cent of the total collision strength. Similar behaviour is seen for the other transitions and convergence is even faster at lower energies.

3 RESULTS AND DISCUSSION

We present collision strengths Ω and thermally averaged effective collision strengths Υ for the optically forbidden transitions among the fine-structure levels of the ground configuration of the O^+ ion. The total collision strength Ω_{ij} is symmetric in i and j, and is given by

$$\Omega_{ij} = \sum_{J\pi} \Omega_{ij}^{J\pi}, \tag{1}$$

where $\Omega_{ij}^{J\pi}$ is a partial collision strength for a transition from an initial target state denoted by $\alpha_i J_i$ to a final target state $\alpha_j J_j$, α_i and α_j being the additional quantum numbers necessary for definition of the target states and sum runs over all partial waves $J\pi$.

The total cross-section for the transition from i to j can be calculated from Ω_{ij} by the relation

$$\sigma_{ij} = \frac{\pi a_0^2}{(2J_i + 1)k_i^2}\Omega_{ij}, \tag{2}$$

where k_i^2 is the scattering electron energy (in Ry) relative to the state i. Note that σ_{ij} is not symmetrical in relation to i and j.

Assuming that the scattering electrons have a Maxwellian velocity distribution, we can compute the dimensionless thermally averaged or effective collision strength Υ_{ij} for a transition $i \rightarrow j$ which relates to $\Omega_{ij}(E_j)$:

$$\Upsilon_{ij}(T) = \int_0^\infty \Omega_{ij}(E_j)\mathrm{e}^{-E_j/kT}\mathrm{d}(E_j/kT), \tag{3}$$

where E_j is the kinetic energy of the outgoing electron, T is the electron temperature, k is Boltzmann's constant and $\Upsilon_{ij} = \Upsilon_{ji}$. Having determined $\Upsilon_{ij}(T)$, one can subsequently obtain the excitation rate coefficient q_{ij} (in cm^3 s^{-1}) which is usually used in astrophysical and plasma applications:

$$q_{ij} = 8.63 \times 10^{-6}(2J_i + 1)^{-1}T^{-1/2}\Upsilon_{ij}(T)\mathrm{e}^{-\Delta E_{ij}/kT}. \tag{4}$$

The corresponding de-excitation rate coefficient q_{ji} is

$$q_{ji} = 8.63 \times 10^{-6}(2J_j + 1)^{-1}T^{-1/2}\Upsilon_{ij}(T), \tag{5}$$

where ΔE_{ij} is the energy difference between the initial state i and the final state j, and T is the electron temperature in K.

3.1 Collision strengths

In the present work, the electron scattering calculation in the external region using a very fine energy mesh of $\Delta E = 2.5 \times 10^{-6}$ Ry is performed for electron energies between the first excitation threshold at 0.244 32 Ry and just above the highest threshold included in the target at 2.101 47 Ry. This fine energy mesh allows us to accurately delineate the resonance structure of the collision strengths. For electron energies above all excitation thresholds up to 15 Ry, a coarse energy mesh of 0.5 Ry is applied.

In Fig. 1, we present collision strengths Ω for transitions from the ground level $2s^22p^3\ ^4S^o_{3/2}$ to the excited levels $^2D^o_{5/2}$, $^2D^o_{3/2}$ $^2P^o_{3/2}$ and $^2P^o_{1/2}$, plus from the $^2D^o_{5/2}$ level to$^2D^o_{3/2}$ of the same configuration. One can clearly see from Fig. 1 that the ratio of collisions strengths $\Omega(^4S^o_{3/2}$–$^2D^o_{5/2})/\Omega(^4S^o_{3/2}$–$^2D^o_{3/2})$ is equal to approximately 1.5 throughout the energy region. This corresponds to the ratio of statistical weights of the upper levels. A similar situation is found for the ratio $\Omega(^4S^o_{3/2}$–$^2P^o_{3/2})/\Omega(^4S^o_{3/2}$–$^2P^o_{1/2})$, which is very close to 2.0, corresponding to the ratio of statistical weights of the levels of the excited-state term $^2P^o$.

3.2 Effective collision strengths

Collision strengths Ω were initially computed for incident electron energies up to 15 Ry. However, our target basis contains the correlation ROs $\overline{3}$p, $\overline{3}$d and $\overline{4}$f, which we find to give rise to pseudo-resonances at energies above 2.9 Ry. Therefore, we can not exploit the complete energy range provided by our continuum ROs for the calculation of Υ. Consequently, for the purpose of computing effective collision strengths, we choose to truncate the collision strengths Ω at a cut-off energy $E_c = 2.5$ Ry. We also computed the effective collision strengths assuming that Ω is constant for $E > E_c$ and equal to the value at that energy. At the upper limit of temperature for the tabulated Υ values, the results of the two approximations differ by no more than 1 per cent for any transition. This gives us confidence that the collision strengths above 2.5 Ry can be neglected safely.

In Table 3, we present the calculated effective collision strengths Υ for transitions among fine-structure levels of the ground configuration $1s^22s^22p^3$ of O II. The level indices denoting a transition correspond to the values of N in Table 1. Effective collision strengths are presented for the temperature range $T = 100{-}100\,000$ K for all transitions involving the five lowest levels of the ground configuration.

As for the collision strengths Ω, the ratio of effective collision strengths $\Upsilon(^4S^o_{3/2}$–$^2D^o_{5/2})/\Upsilon(^4S^o_{3/2}$–$^2D^o_{3/2})$ for the transitions 1–2 and 1–3 remains constant, and equals to about 1.5. Hence, we do not detect any deviation from the ratio of statistical weights of the upper levels, as found in the results of McLaughlin & Bell (1998). This is also the case for the ratio for the lines 1–4 and 1–5, which is very close to 2.0 and corresponds to the ratio of the statistical weights of the upper levels $^2P^o_{3/2}$ and $^2P^o_{1/2}$.

3.3 Energy mesh for collision strengths

It is very important to use an energy mesh ΔE which will enable us to delineate all important resonance structure. Since there are resonances in the collision strengths very close to the excitation thresholds (see Fig. 1), a mesh which is not sufficiently fine could lead to some inaccuracies when effective collision strengths Υ are computed, especially at the lower end of the electron temperature range.

We have calculated collision strengths for different values of the energy mesh ΔE in order to ensure the convergence of our data. A comparison of effective collision strengths (Υ) is presented in Table 4. In this table, we list data for transitions among the three lowest fine-structure levels of the configuration $1s^22s^22p^3$, obtained by employing four different values of energy mesh, the coarsest one being $\Delta E = 2 \times 10^{-5}$ Ry and the finest one being $\Delta E = 2.5 \times 10^{-6}$ Ry. Values for Υ are presented for the transitions which have resonances lying close to the first excitation threshold. For other transitions, agreement is even better than for the ones presented here.

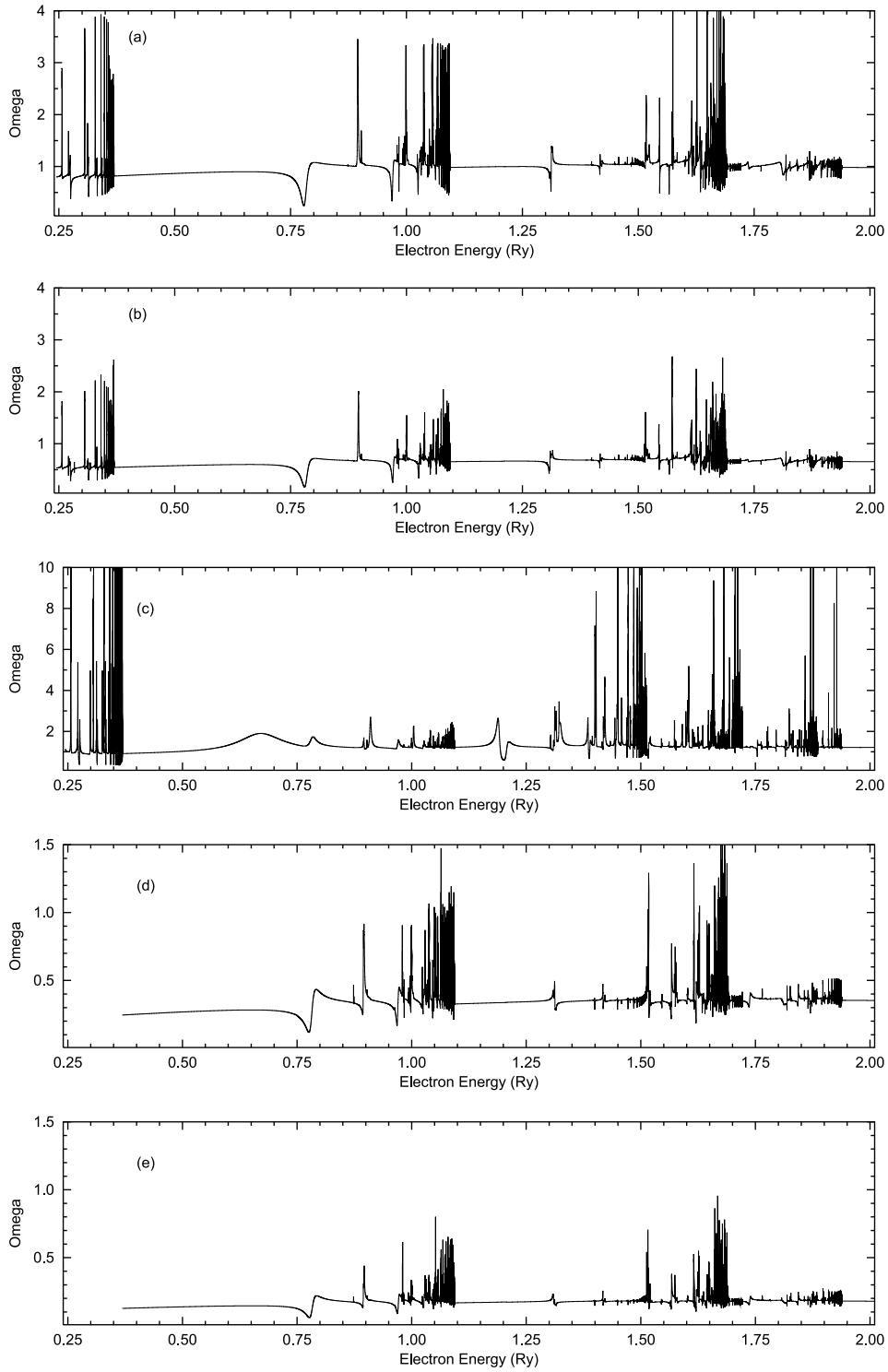

Figure 1. Collision strengths for transitions among the fine-structure levels of the ground configuration $1s^2 2s^2 2p^3$ of O II; (a) $^4S^o_{3/2}$–$^2D^o_{5/2}$, (b) $^4S^o_{3/2}$–$^2D^o_{3/2}$, (c) $^2D^o_{5/2}$–$^2D^o_{3/2}$, (d) $^4S^o_{3/2}$–$^2P^o_{3/2}$, (e) $^4S^o_{3/2}$–$^2P^o_{1/2}$. Electron energies are in Rydbergs relative to the lowest level $^4S^o_{3/2}$.

One can see from Table 4 that the convergence of effective collision strengths Υ with regard to energy mesh is achieved. Any notable difference in Υ does not exceed 4 per cent at the very low electron temperatures, and it is negligible for temperatures above 1000 K. Consequently, we are sure that the energy mesh ΔE applied in our calculation is sufficiently fine to properly delineate the resonance structure in the collision strengths, and that it does not lead to any substantial inaccuracies in our computed data for effective collision strengths.

3.4 Comparison with other data

In addition to examining the influence of the energy mesh employed in our calculation, we wish to examine how the choice of different CI expansions for the target states and different RO sets affects

Table 3. Effective collision strengths Υ for transition among fine-structure levels of the ground configuration $1s^2 2s^2 2p^3$ in O II.

T (K)	1−2	1−3	1−4	1−5	2−3
100	0.796	0.531	0.244	0.126	1.095
150	0.797	0.533	0.245	0.126	1.086
200	0.798	0.533	0.245	0.126	1.078
300	0.801	0.535	0.245	0.126	1.072
500	0.808	0.540	0.245	0.127	1.097
750	0.817	0.546	0.246	0.127	1.151
1000	0.823	0.550	0.246	0.127	1.194
1500	0.830	0.554	0.247	0.127	1.239
2000	0.832	0.555	0.247	0.128	1.254
3000	0.832	0.554	0.249	0.128	1.256
5000	0.831	0.553	0.251	0.129	1.241
7500	0.833	0.553	0.253	0.131	1.221
10 000	0.834	0.554	0.256	0.132	1.203
15 000	0.839	0.557	0.260	0.134	1.183
20 000	0.844	0.561	0.265	0.136	1.179
30 000	0.856	0.569	0.274	0.141	1.193
50 000	0.881	0.585	0.290	0.149	1.229
75 000	0.905	0.601	0.304	0.155	1.257
100 000	0.919	0.611	0.312	0.159	1.270
T (K)	2−4	2−5	3−4	3−5	4−5
100	0.791	0.315	0.439	0.308	0.273
150	0.793	0.316	0.440	0.308	0.274
200	0.793	0.316	0.440	0.309	0.274
300	0.794	0.316	0.440	0.309	0.274
500	0.796	0.317	0.441	0.310	0.274
750	0.797	0.318	0.442	0.310	0.275
1000	0.799	0.318	0.443	0.311	0.275
1500	0.801	0.319	0.444	0.312	0.276
2000	0.804	0.320	0.445	0.313	0.276
3000	0.809	0.322	0.448	0.315	0.277
5000	0.820	0.326	0.454	0.319	0.279
7500	0.834	0.332	0.462	0.324	0.282
10 000	0.851	0.339	0.472	0.331	0.285
15 000	0.891	0.356	0.494	0.345	0.294
20 000	0.930	0.371	0.516	0.360	0.305
30 000	0.997	0.396	0.551	0.386	0.327
50 000	1.084	0.427	0.595	0.421	0.361
75 000	1.144	0.447	0.624	0.445	0.388
100 000	1.178	0.458	0.639	0.459	0.405

the computed collision strengths and effective collision strengths. Additionally, we wish to investigate how the use of the experimental target energies in the R-matrix calculations can influence the results.

In Table 5, we present the effective collision strengths Υ obtained using different configuration and target energy sets, and compare our results with available data from other authors. One set of data is obtained using adjusted (to the experimental) target energies. The target level energy corrections $\Delta E_{\rm TFD}$, $\Delta E_{\rm TFD1}$ and $\Delta E_{\rm STO1}$ in this type of calculation for the different sets of ROs are presented in Table 1. In another set of calculations, the pure theoretical results of the *ab initio* energy levels are used, without any adjustment being applied to the target level energies.

For each set of target level energies, we have performed three series of calculations. In the calculation denoted as TFD, we use the most extensive set of configurations in the target wavefunction CI expansion, which is given in Section 2.1, based on Thomas–Fermi–Dirac-type ROs. TFD1 uses a smaller wavefunction CI expansion (see Section 2.1) with the same radial TFD-type orbitals. The third calculation STO1 uses the same configuration set as TFD1, but

Table 4. Comparison of effective collision strengths Υ for transitions among the ground configuration $1s^2 2s^2 2p^3$ levels of O II, calculated using the TFD ROs and the experimental target energies for various energy meshes; h_1: $\Delta E = 2 \times 10^{-5}$ Ry, h_2: $\Delta E = 1 \times 10^{-5}$ Ry, h_3: $\Delta E = 5 \times 10^{-6}$ Ry, h_4: $\Delta E = 2.5 \times 10^{-6}$ Ry.

T (K)	h_1	h_2	h_3	h_4
		$^4S^o_{3/2}-{}^2D^o_{5/2}$		
100	0.774	0.786	0.792	0.796
150	0.783	0.791	0.795	0.797
200	0.787	0.794	0.797	0.798
300	0.793	0.798	0.800	0.801
500	0.803	0.806	0.807	0.808
1000	0.821	0.822	0.823	0.823
2000	0.831	0.831	0.832	0.832
10 000	0.834	0.834	0.834	0.834
100 000	0.919	0.919	0.919	0.919
		$^4S^o_{3/2}-{}^2D^o_{3/2}$		
100	0.517	0.525	0.529	0.531
150	0.523	0.528	0.531	0.533
200	0.526	0.530	0.532	0.533
300	0.530	0.533	0.534	0.535
500	0.537	0.538	0.539	0.540
1000	0.549	0.549	0.550	0.550
2000	0.554	0.554	0.554	0.555
10 000	0.554	0.554	0.554	0.554
100 000	0.611	0.611	0.611	0.611
		$^2D^o_{5/2}-{}^2D^o_{3/2}$		
100	1.064	1.082	1.090	1.095
150	1.065	1.077	1.083	1.086
200	1.063	1.072	1.076	1.078
300	1.061	1.067	1.070	1.072
500	1.090	1.094	1.096	1.097
1000	1.191	1.193	1.194	1.194
2000	1.252	1.253	1.254	1.254
10 000	1.201	1.205	1.205	1.203
100 000	1.269	1.271	1.271	1.270

employs Slater-type ROs as a basis. This type of calculation is the closest one to that performed by McLaughlin & Bell (1998).

We compare our data for Υ with the results of Montenegro et al. (2006) which we denote as BPRM06. Their close-coupling calculation was performed in the Breit-Pauli approximation using the R-matrix codes. The results given by Tayal (2007) obtained by using a 47-level Breit-Pauli R-matrix approach with non-orthogonal radial functions are presented in the column T07. In addition, we include data from McLaughlin & Bell (1998), denoted as MB98, for comparison in the last column of Table 5. There are two main differences between our calculation and that of Montenegro et al. (2006): (i) they used a smaller CI expansion of the target, six configurations compared to our 22; (ii) their 3p and 3d radial functions were real physical orbitals, whereas ours are correlation orbitals optimized to improve the representation of the $2s^2 2p^3$ and $2s2p^4$ levels.

When comparing our results obtained using the experimental target energies but different sets of configuration expansion and different ROs, we can see that the values for Υ show no substantial differences. The TFD and TFD1 data almost exactly match, while the STO1 results differ by a few per cent at lower temperatures for the transitions originating from the ground level $^4S^o_{3/2}$. There are minor differences in the effective collision strengths for the $^2D^o_{5/2} - {}^2D^o_{3/2}$ transition at very low electron temperatures, but this becomes negligible for $T \geq 5000$ K.

Table 5. Comparison of the effective collision strengths Υ for transitions among the ground configuration $1s^2 2s^2 2p^3$ levels in O II, calculated using different configuration sets, different ROs, experimental and theoretical level energies, with the BP calculations of Montenegro et al. (2006) denoted as BPRM06, McLaughlin & Bell (1998) denoted as MB98 and Tayal (2007) denoted as T07.

	Experimental level energies			Theoretical level energies			Other calculation		
T (K)	TFD	TFD1	STO1	TFD	TFD1	STO1	BPRM06	T07	MB98
					$^4S^o_{3/2}-^2D^o_{5/2}$				
200	0.798	0.791	0.778	0.794	0.812	1.034			
500	0.808	0.802	0.787	0.797	0.826	0.961			
1000	0.823	0.818	0.802	0.805	0.841	0.909	0.864		
5000	0.831	0.828	0.812	0.828	0.837	0.848	0.885	0.798	0.81
10 000	0.834	0.830	0.815	0.835	0.837	0.846	0.883	0.803	0.82
20 000	0.844	0.837	0.823	0.846	0.843	0.852	0.885	0.813	0.84
100 000	0.919	0.911	0.898	0.922	0.908	0.921		0.874	0.94
					$^4S^o_{3/2}-^2D^o_{3/2}$				
200	0.533	0.529	0.519	0.529	0.541	0.705			
500	0.540	0.536	0.526	0.532	0.551	0.656			
1000	0.550	0.547	0.536	0.538	0.563	0.616	0.590		
5000	0.553	0.550	0.539	0.553	0.558	0.568	0.587	0.548	0.41
10 000	0.554	0.551	0.541	0.559	0.560	0.567	0.585	0.550	0.43
20 000	0.561	0.557	0.547	0.566	0.564	0.571	0.585	0.553	0.44
100 000	0.611	0.605	0.597	0.614	0.604	0.613		0.585	0.49
					$^4S^o_{3/2}-^2P^o_{3/2}$				
200	0.245	0.245	0.251	0.248	0.258	0.250			
500	0.245	0.246	0.252	0.249	0.258	0.250			
1000	0.246	0.246	0.252	0.249	0.259	0.251	0.299		
5000	0.251	0.251	0.257	0.254	0.263	0.255	0.307	0.279	0.25
10 000	0.256	0.256	0.261	0.259	0.267	0.260	0.313	0.283	0.26
20 000	0.265	0.264	0.269	0.268	0.274	0.268	0.322	0.288	0.27
100 000	0.312	0.309	0.310	0.314	0.313	0.313		0.315	0.33
					$^4S^o_{3/2}-^2P^o_{1/2}$				
200	0.126	0.126	0.131	0.128	0.129	0.134			
500	0.127	0.127	0.131	0.128	0.129	0.134			
1000	0.127	0.127	0.132	0.129	0.129	0.135	0.148		
5000	0.129	0.129	0.134	0.131	0.131	0.137	0.151	0.138	0.11
10 000	0.132	0.132	0.136	0.133	0.134	0.139	0.152	0.140	0.12
20 000	0.136	0.136	0.139	0.138	0.138	0.142	0.156	0.142	0.12
100 000	0.159	0.158	0.159	0.161	0.160	0.160		0.157	0.15
					$^2D^o_{5/2}-^2D^o_{3/2}$				
200	1.078	1.145	1.261	1.289	1.035	3.560			
500	1.097	1.145	1.218	1.709	1.138	2.574			
1000	1.194	1.231	1.270	1.699	1.275	1.957	1.618		
5000	1.241	1.258	1.255	1.404	1.273	1.349	1.518	1.653	1.52
10 000	1.203	1.211	1.202	1.298	1.218	1.250	1.426	1.434	1.25
20 000	1.179	1.176	1.158	1.234	1.179	1.200	1.324	1.291	1.17
100 000	1.270	1.260	1.241	1.281	1.255	1.274		1.260	1.24

For the results obtained using the *ab initio* target levels energies, the situation is quite different. There are notable discrepancies in the values of Υ for the different configuration expansion sets and different ROs. This is particularly true for $^4S^o_{3/2}-^2D^o_{5/2}$, $^4S^o_{3/2}-^2D^o_{3/2}$ and $^2D^o_{5/2}-^2D^o_{3/2}$, and for low electron temperatures. There is much better agreement at higher temperatures for these transitions as well as for $^4S^o_{3/2}-^2P^o_{3/2}$ and $^4S^o_{3/2}-^2P^o_{1/2}$, where the discrepancies in Υ are very small at all temperatures. Results obtained using the theoretical target level energies are generally consistent, and agree with the data obtained using the experimental target energies. Differences are due to the resonances positioned very close to the excitation threshold. Their position depends on the type of ROs used and on the CI expansion applied (see Table 1).

For illustrative purposes, we present a plot of the near-threshold collision strengths Ω for $^2D^o_{5/2}-^2D^o_{3/2}$ obtained within the STO1 set, using both the experimental (solid line) and the theoretical (dashed line) target level energies in Fig. 2. It is clear that the first resonance structure is located right on the edge of the excitation threshold, at 0.265 19 Ry (see Table 1) in the case of the theoretical target energies. However, the same resonance structure is shifted away from the threshold by more than 0.01 Ry when energy adjustments are introduced. Even if the background value of collision strength does not depend on the type of target energies used (as may be seen from Fig. 2), the low electron temperature behaviour of the effective collision strength Υ is defined by the near-threshold resonances and their positions.

When the electron temperature increases, the low-energy part of the collision strength Ω becomes less important in the overall value of Υ, and the agreement of the different sets of effective collision strengths Υ becomes significantly better. This points to

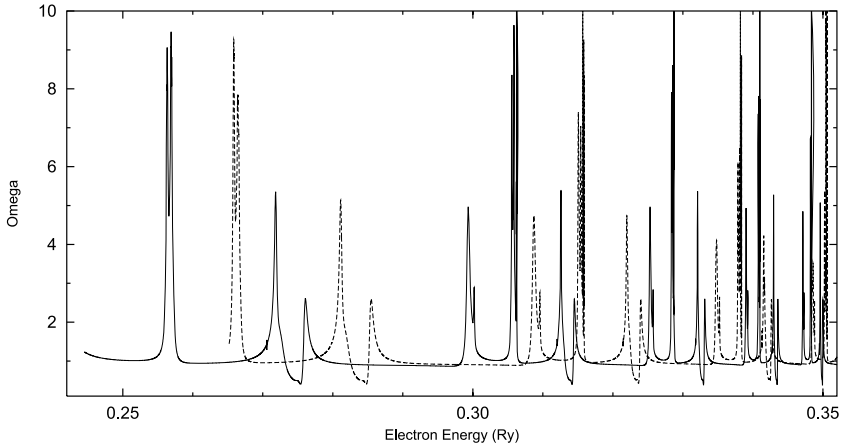

Figure 2. Collision strengths for the transition $^2D^o_{5/2}-^2D^o_{3/2}$ in O II near the excitation threshold. Electron energies are in Rydbergs relative to the ground level $^4S^o_{3/2}$. The solid line is for the calculation with adjusted target level energies, while the dashed line is for data with *ab initio* level energies.

the fact that collision strength background values are essentially the same for both the experimental and theoretical target level energies. Hence, introducing the target-energy adjustments changes only the positions of resonances. Therefore, these adjustments cannot lead to substantial deviations for the calculated effective collision strengths, especially at the higher electron temperatures.

A comparison with the Breit-Pauli results (BPRM06) of Montenegro et al. (2006) and Pradhan et al. (2006) indicates reasonable agreement, although our Υ values are consistently smaller than their values. For the transition $^4S^o_{3/2}-^2D^o_{5/2}$, the difference is 4–5 per cent, for $^4S^o_{3/2}-^2D^o_{3/2}$ is 5–8 per cent, for $^4S^o_{3/2}-^2P^o_{3/2}$ is around 20 per cent and for $^4S^o_{3/2}-^2P^o_{1/2}$ is 15–17 per cent. These discrepancies are caused by the different background values of the corresponding collision strengths Ω, arising from the different configuration expansion sets used in our calculation and in those of Montenegro et al. (2006).

A slightly more complicated situation is observed for $^2D^o_{5/2}-^2D^o_{3/2}$, where the discrepancy in Υ is 36 per cent at $T = 1000$ K, which falls to just 12 per cent at $T = 20\,000$ K. We can attribute the larger discrepancy of the low temperature results to differences in the resonance structure of the collision strengths positioned right on the excitation threshold of this transition, which is notable in fig. 1 from Pradhan et al. (2006). The discrepancies at higher temperatures are for the same reason as for the transitions originating from the ground level $2s^22p^3\ ^4S^o_{3/2}$.

A similar pattern can be observed for transitions originating from the levels $^2D^o_{5/2}$ and $^2D^o_{3/2}$, where differences in the calculated values of Υ remain approximately constant, and are largely due to the differing background values. When we compare effective collision strength ratios for the transitions originating from the ground level $^4S^o_{3/2}$, we see that they are very close to the ratios of the statistical weights of the upper levels. At $T = 10\,000$ K, the ratio $\Upsilon(^4S^o_{3/2}-^2D^o_{5/2})/\Upsilon(^4S^o_{3/2}-^2D^o_{3/2})$ is 1.505 in our calculation and 1.509 in that of Pradhan et al. (2006), while the ratio $\Upsilon(^4S^o_{3/2}-^2P^o_{3/2})/\Upsilon(^4S^o_{3/2}-^2P^o_{1/2})$ is 1.94 and 2.06, respectively. Although for transitions originating from $^2D^o_{5/2}$ and $^2D^o_{3/2}$ to $^2P^o_{3/2}$ and $^2P^o_{1/2}$, the ratio of Υ does not correspond to the ratio of the upper level statistical weights, it is approximately the same both in our calculation and in that of BPRM06.

A comparison with data of Tayal (2007) presented in the column T07 of Table 5 indicates very good agreement. For the transitions $^4S^o_{3/2}-^2D^o_{5/2}$, $^2D^o_{3/2}$, the differences in Υ values do not exceed few per cent, with our results being slightly higher. For the transitions to the levels $^2P^o_{3/2}$ and $^2P^o_{1/2}$, our calculated effective collision strengths are slightly smaller than those of Tayal (2007). A similar pattern is observed for the forbidden transitions not only from the ground level but also from the excited levels of the multiplets ^2D and ^2P. However, we note that the results for the excitation to the levels $^2P^o_{3/2}$ and $^2P^o_{1/2}$ in table 3 of Tayal (2007) should be swapped to obtain the correct data. This was probably due to the fact that the energy ordering for the corresponding calculated levels differs from the experimental one. The effective collision strengths for the transition $^2D^o_{5/2}-^2D^o_{3/2}$ differ significantly, the deviation reaching some 25 per cent at the lower temperature end. It should be noted that the differences are smaller when the theoretical level energies are employed in our calculations, suggesting that the main reason for this disagreement is that we use experimental level energies in our scattering calculation leading to more accurate data. This is particularly important for the transition $^2D^o_{5/2}-^2D^o_{3/2}$ because of resonance structures present very close to the excitation threshold (see Fig. 2).

A comparison of our data (from the TFD set) with the BP calculations of McLaughlin & Bell (1998) reveals two different trends. For some transitions, namely $^4S^o_{3/2}-^2D^o_{5/2}$ and $^4S^o_{3/2}-^2P^o_{3/2}$, the agreement is exceptionally good, even better than the Montenegro et al. (2006) data. This is due to the similar target and wavefunction CI expansion used. For $^2D^o_{5/2}-^2D^o_{3/2}$, the effective collision strengths agree very well at higher electron temperatures, whereas some difference appears at $T = 5000$ K, which can be attributed to the effect of the near-threshold resonances.

For other transitions from the ground state, shown in Table 5, there are very significant discrepancies between our effective collision strengths and those of McLaughlin & Bell (1998). The data differ by nearly 30 per cent for excitation to the $^2D^o_{3/2}$ level and by 15–20 per cent for the $^2P^o_{1/2}$ level. It is worth noting that both of these are the upper levels of their corresponding terms, ^2D or ^2P, respectively. Such a large drop in the value of the effective collision strength Υ causes the significant deviation from the statistical-weight ratio, which is not expected for a singly ionized ion with $Z = 8$. McLaughlin & Bell explain this effect by the influence of configuration mixing, but there are no data presented in their work to confirm such a conclusion.

Checking our CI wavefunction expansion coefficients for the fine-structure levels of the $1s^22s^22p^3$ configuration, we do not find

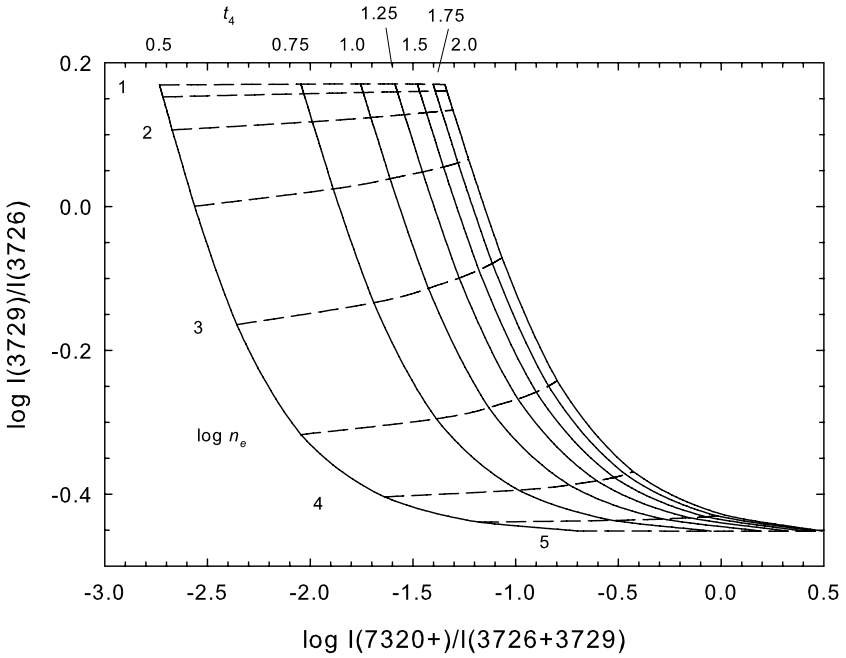

Figure 3. Ratio–ratio diagram for O II transitions, where I is in energy units, computed using the new collision strengths and the transition probabilities described in the text. The electron density n_e is in units of cm^{-3}, while the electron temperature t_4 is in units of 10^4 K.

any substantial configuration mixing effects which can cause this kind of deviation. The main contributing term is usually more than 0.95 for levels with $J = 3/2$ and approximately 0.99 for levels with $J = 1/2$. These appear to be very reasonable values for a low-Z ion. Therefore, we conclude that the data of McLaughlin & Bell (1998) for some transitions are incorrect. Although we cannot define any particular reason for the inaccuracy of their data, the most plausible cause is a limited CI expansion of the target wavefunctions, where an incomplete set of CSFs is used.

4 CONCLUSIONS

In the current work, we have determined the collision strengths Ω and the effective collision strengths Υ for a wide range of electron temperatures T using the relativistic Breit-Pauli R-matrix code for the excitation of forbidden lines among the fine-structure levels of the ground configuration $1s^2 2s^2 2p^3$ of the O^+ ion. The collision strengths are calculated using a very fine energy mesh, which allows the delineation of all resonance structure to high accuracy. A comparison of the effective collision strengths obtained using different energy meshes confirms that a convergence of Ω on the energy mesh was achieved.

The collision strengths are computed using various target wavefunction expansions and different sets of the ROs, employing both the *ab initio* theoretical and experimental energies for the target levels. In all cases, we do not detect any sizeable difference in the background value of the calculated Ω.

In all six data sets for our calculations, we do not find any significant departure from the statistical distribution for the ratio of the collision strengths Ω and the effective collision strengths Υ. This confirms the findings of Montenegro et al. (2006), and shows that the results of McLaughlin & Bell (1998) for some transitions are inaccurate. Although we have tried to replicate the latter calculation and establish the origin of the departure of their results from the statistical-weight rule, we did not find any reason why it could happen.

Consequently, any analysis of observations based on the atomic data from McLaughlin & Bell (1998) must be treated with caution. The differences between our results and those of Montenegro et al. (2006) and Pradhan et al. (2006) can be attributed to the more extensive and converged CI expansion used here, and we therefore consider the results given in Table 3 to be the best available for this ion at present.

The revised rates will change the plasma diagnostics presented by Keenan et al. (1999). We have therefore regenerated the O II line ratios and shown some results in Fig. 3. These employ the transition probabilities given by Zeippen (1982) since these are in better agreement with observations (Wang et al. 2004). We refer the reader to Keenan et al. (1999) for further details, and to compare how the new collision rates have changed the results.

ACKNOWLEDGMENTS

Support for proposal HST-AR-09923 was provided by NASA through a grant from the Space Telescope Science Institute, which is operated by the Association of Universities for Research in Astronomy, Inc., under NASA contract NAS5-26555. FPK is grateful to AWE Aldermaston for the award of a William Penney Fellowship. This work was supported by STFC and EPSRC, and also by NATO Collaborative Linkage Grant CLG.979443. We are also grateful to the Defence Science and Technology Laboratory (dstl) for support under the Joint Grants Scheme. GJF thanks the NSF (AST 0607028), NASA (NNG05GD81G), STScI (HST-AR-10653) and the *Spitzer* Science Center (20343) for support. We acknowledge the use of software from the Condor Project (http://www.condorproject.org/) in running the R-matrix codes.

REFERENCES

Bell K. L., Burke P. G., Hibbert A., Kingston A. E., 1989, J. Phys. B, 22, 3197

Bell K. L., Hibbert A., Stafford R. P., McLaughlin B. M., 1994, Phys. Scripta, 50, 343
Berrington K. A., Burke P. G., Butler K., Seaton M. J., Storey P. J., Taylor K. T., Yan Y., 1987, J. Phys. B, 20, 6379
Berrington K. A., Eissner W., Norrington P. H., 1995, Comput. Phys. Commun., 92, 920
Burke P. G., Robb W. D., 1975, Adv. At. Mol. Phys., 11, 143
Copetti M. V. F., Writzl B. C., 2002, A&A, 382, 282
Eissner W., Jones M., Nussbaumer H., 1974, Comput. Phys. Commun., 15, 23
Hibbert A., 1975, Comput. Phys. Commun., 9, 141
Keenan F. P., Aller L. H., Bell K. L., Crawford F. L., Feibelman W. A., Hyung S., McKenna F. C., McLaughlin B. M., 1999, MNRAS, 304, 27
McLaughlin B. M., Bell K. L., 1998, J. Phys. B, 31, 4317
Montenegro M., Eissner W., Nahar S. N., Pradhan A. K., 2006, J. Phys. B: At. Mol. Opt. Phys., 39, 1863
Nussbaumer H., Storey P. J., 1978, A&A, 64, 139
Osterbrock D. E., 2000, ARA&A, 38, 1
Osterbrock D. E., Ferland G. J., 2006, in Osterbrock D. E., Ferland G. J., eds, Astrophysics of Gaseous Nebulae and Active Galactic Nuclei, 2nd edn. University Science Books, Sausalito, CA
Pradhan A. K., 1976, MNRAS, 177, 31
Pradhan A. K., Montenegro M., Nahar S. N., Eissner W., 2006, MNRAS, 366, L6
Scott N. S., Burke P. G., 1980, J. Phys. B, 13, 4299
Seaton M. J., 1987, J. Phys. B, 20, 6363
Seaton M. J., Osterbrock D. E., 1957, ApJ, 125, 66
Tayal S. S., 2006, J. Phys. B: At. Mol. Opt. Phys., 39, 4393
Tayal S. S., 2007, ApJS, 171, 331
Wang W., Liu X.-W., Zhang Y., Barlow M. J., 2004, A&A, 427, 873
Wenåker I., 1990, Phys. Scripta, 42, 667
Zeippen C. J., 1982, MNRAS, 198, 111

This paper has been typeset from a TEX/LATEX file prepared by the author.